



City Research Online

City, University of London Institutional Repository

Citation: Thomaidis, I., Camara Casado, A. & Kappos, A. (2022). Dynamics and seismic performance of asymmetric rocking bridges. *Journal of Engineering Mechanics*, 148(3), 04022003. doi: 10.1061/(asce)em.1943-7889.0002074

This is the accepted version of the paper.

This version of the publication may differ from the final published version.

Permanent repository link: <https://openaccess.city.ac.uk/id/eprint/27069/>

Link to published version: [https://doi.org/10.1061/\(asce\)em.1943-7889.0002074](https://doi.org/10.1061/(asce)em.1943-7889.0002074)

Copyright: City Research Online aims to make research outputs of City, University of London available to a wider audience. Copyright and Moral Rights remain with the author(s) and/or copyright holders. URLs from City Research Online may be freely distributed and linked to.

Reuse: Copies of full items can be used for personal research or study, educational, or not-for-profit purposes without prior permission or charge. Provided that the authors, title and full bibliographic details are credited, a hyperlink and/or URL is given for the original metadata page and the content is not changed in any way.

DYNAMICS AND SEISMIC PERFORMANCE OF ASYMMETRIC ROCKING BRIDGES

Ioannis M. Thomaidis¹, Alfredo Camara¹, and Andreas J. Kappos²

¹School of Mathematics, Computer Science and Engineering, City, University of London, London, United Kingdom

²Department of Civil Infrastructure and Environmental Engineering, Khalifa University, Abu Dhabi, United Arab
Emirates

ABSTRACT

The governing equations of motion for bridges with rocking piers of unequal height and unequal span lengths are derived accounting for the effect of end joint gaps and the abutment-backfill system. The attenuation of the rocking motion stems from the impacts at the rocking interfaces, described through the coefficient of restitution, and also from the impacts (pounding) of the superstructure on the abutment backwalls. This is the first study that combines both energy dissipation sources in the analytical derivation of the equations of motion. The results of response-history analysis of bridges with different levels of asymmetry in their pier height show that the performance of both the symmetric and asymmetric configurations is very similar with regard to longitudinal displacements. Although the studied bridges safely resisted ground motions with an intensity about twice that of the design earthquake, regardless of the degree of asymmetry, it was found that the higher the difference in the pier height, the larger is the rotation of the superstructure due to the differential uplift of the piers, a point that has to be addressed in seismic design for rocking response.

KEYWORDS

Rocking bridges, unequal pier height, asymmetry, abutment, backfill, analytical methods, rigid body dynamics

Cite as:
Thomaidis IM, **Camara A** and Kappos AJ (2021). Dynamics and seismic performance of asymmetric rocking bridges. *Journal of Engineering Mechanics*. Currently in Press.

INTRODUCTION

The seismic response of structures with rocking piers is characterized by a sequence of self-centering rigid body rotations that are combined with dissipative impacts each time the structure returns to the original position of equilibrium, and it continues until the total energy is dissipated through these impacts; this system is characterized by a highly nonlinear behavior. The first systematic study on the topic was published by Housner (1963) who developed a simple analytical two-dimensional (2D) model that has been extensively validated (Bachmann et al. 2018, Thomaidis et al. 2018 and Ceh et al. 2018). Thereafter, a number of studies have addressed the dynamic response of rocking columns and established the high stability of this simple configuration (see i.a. Makris and Roussos 2000, Makris and Zhang 2001, Dimitrakopoulos and DeJong 2012, Vassiliou and Makris 2012, Acikgoz and DeJong 2014, Vassiliou and Makris 2015, Makris and Kampas 2016, Thiers-Moggia and Malaga-Chuquitaype 2018).

Other authors studied the seismic response of frames wherein the columns have the same section (both in elevation and cross-section) and height, as is common in ancient monuments (see i.a. Psycharis et al. 2000, Drosos and Anastasopoulos 2014). Makris and Vassiliou (2013) developed the Equation of Motion (EoM) of a beam supported on an infinite number of equal-height columns (symmetric or regular configuration), as well as the energy dissipation at the impacts at the rocking interfaces using the concept of the Coefficient of Restitution (CoR). However, real bridges usually have piers of different heights to accommodate the topography of the site. To account for this, DeJong and Dimitrakopoulos (2014) and Dimitrakopoulos and Giouvanidis (2015) studied the dynamics of a frame supported on two rocking columns with same section but different height (asymmetric or irregular configuration). In both studies the concept of CoR was utilized for the impact at the rocking interfaces. These works do not address the effect of the abutment-backfill system, which was found to be significant in the rocking response of symmetric bridges by Thomaidis et al. (2020a) due not only to the longitudinal constraint to the deck movement, but also to the vertical impacts between the deck and the abutment seats. Different failure modes were observed in the response of rocking bridges when the effects of the abutment-backfill are considered, but to the authors' knowledge this has not been considered in analytical studies of bridges with unequal pier heights. Developing the EoM and exploring the seismic response of asymmetric/irregular rocking bridges is the aim of the present study.

The dynamics of asymmetric bridges with two rocking piers of different height are studied here by extending the analytical models of Dimitrakopoulos and Giouvanidis (2015) and Thomaidis et al. (2020a) to account for the abutment-backfill (not included in the former study) and the pier asymmetry (not addressed in the latter). The EoM

accounts for the difference in the spans, the presence of end joints, and the longitudinal and vertical effects of the deck support at the abutment seats. The CoR in this general case is derived following the ‘classical’ impulse formulation but incorporating a new inherent energy dissipation mechanism to describe the impact of the superstructure on the abutment backwall by means of an additional CoR. The proposed formulation is used to analyze the response of asymmetric rocking bridges subject to high intensity ground motions, and it assesses their seismic behaviour with a view to establishing the effect of asymmetry in rocking bridges.

ANALYTICAL MODEL OF THE ROCKING RESPONSE OF ASYMMETRIC BRIDGES

This section presents an analytical model to describe the longitudinal rocking motion of straight bridges supported by two piers with the same section and different heights, and by seat-type abutments, accounting not only for the vertical support at the abutment seat, but also for the activation of the abutment-backfill system when the end gap closes. Fig. 1 illustrates the general bridge configuration at the at-rest position, subject to a horizontal ground acceleration history \ddot{u}_g . The deck consists of a continuous box girder section with depth $2h$, cross-sectional area A_{deck} and total length $L_{tot} = 2L_1 + L_2$, with L_1 and L_2 being the side and central spans, respectively. The deck is free to move longitudinally until the joint gap between one of its ends and the abutment is closed (u_{jo}). At this instant, an impact on the abutment backwall with height h_{bw} occurs. The superstructure is supported on frictionless sliding bearings at the abutment seats E and E' that can accommodate the up-and-down (cyclic vertical) motion of the superstructure; this selection is conservative in the context of a performance assessment considering that the superstructure is not restrained and, therefore, the prevailing failure mode of the abutment-backfill system (see discussion below) can be activated more easily. The two free-standing rocking piers have a width $2B$ and unequal heights $2H_1$ and $2H_2$ for the tall and short pier, respectively. The semi-diagonals of the piers are given by $R_1 = \sqrt{H_1^2 + B^2}$ and $R_2 = \sqrt{H_2^2 + B^2}$, while the slenderness parameters are $\alpha_1 = \tan^{-1}(B/H_1)$ and $\alpha_2 = \tan^{-1}(B/H_2)$, respectively. Special grooved caps are introduced at the bottom and the top surfaces of both piers to allow free rocking on the base (pivot points A'-A for the tall pier and C'-C for the short pier) and the deck interfaces (pivot points B-B' and D-D'). Two additional parameters are used in the analytical formulation of the asymmetric bridge rocking motion, namely the distance between the pivot points of the piers at the foundation level $2r_{AC} = \sqrt{(2H_1 - 2H_2)^2 + L_2^2}$, and the angle between this line and the horizontal $\phi_{AC} = \tan^{-1}((2H_1 - 2H_2)/L_2)$.

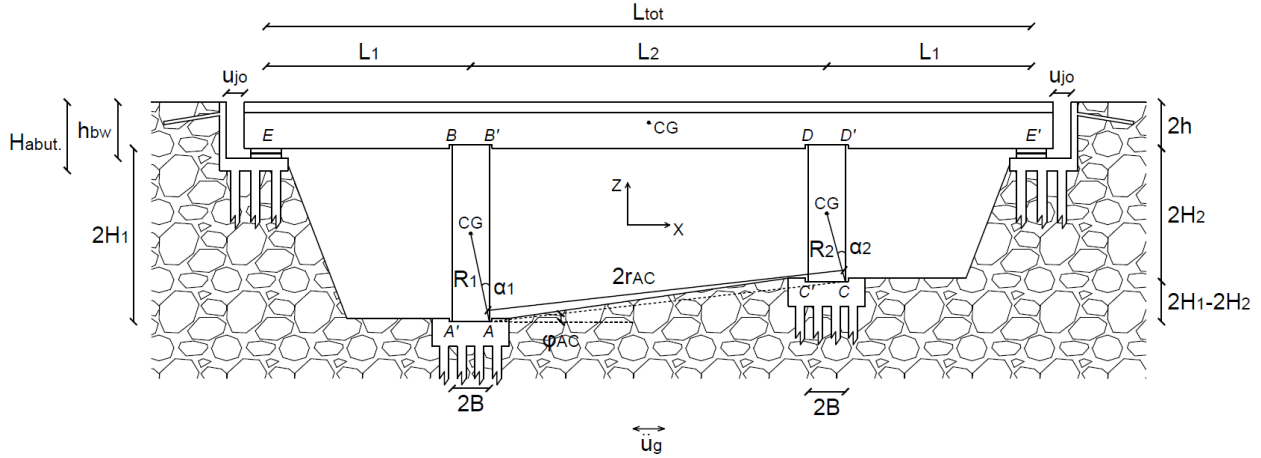


Fig. 1. Schematic of an asymmetric bridge (at the at-rest position) supported on two rectangular-in-elevation free-standing rocking piers, and frictionless sliding bearings at the abutment seats.

The following assumptions are adopted to formulate the rocking motion of the asymmetric bridge structure:

- The rocking motion is constrained within the plane of the bridge, thus ignoring three-dimensional (3D) rocking response (Chatzis and Smyth 2012a, Vassiliou 2017).
- The deformability of all structural members is ignored (rigid body dynamics), without a significant loss of accuracy, as shown i.a. by Agalianos et al. (2017) and Thomaidis et al. (2020b).
- The piers are designed to rock freely on the foundation (pivots A'-A and C'-C) and the deck interfaces (pivots B-B' and D-D'), without sliding at the initiation of movement, as shown for free-standing rocking columns by Taniguchi (2002), and throughout the entire motion. This can be achieved by means of grooves provided on the top surface of the foundation and at the soffit of the deck, and it prevents slide-rock movement (Taniguchi 2002, and Jeong et al. 2003).

Fig. 2A, B illustrate the rocking motion of the asymmetric bridge for counter-clockwise (positive, superscript p) and clockwise (negative, superscript n) rotations, respectively. The effect of the abutment and the backfill at each end of the bridge is modelled with a Kelvin-Voigt system (spring (k) and dashpot (c) elements in parallel).

Despite the apparent complexity of the longitudinal rocking motion, it can be described by a single Degree of Freedom (DoF). This is selected as the angle φ formed between the horizontal axis (X) and the diagonal of the tall pier (starting from the pivot point at its base). Consequently, the relative rocking rotation of the tall pier (θ_1) is given by the following expression

$$\theta_1 = \varphi - \varphi_1^{p/n}, \quad (1)$$

where $\varphi_1^{p/n} = \pi/2 \mp \alpha_1$ represents the angle of the tall pier diagonal with respect to the horizontal at the at-rest position. It is noted that the diagonal that is required for determining φ_1^p and φ_1^n is different depending on the direction of the movement and, therefore, it is determined in each case by the pivot points that drive the rocking motion of the tall pier, as shown in Fig. 2. This is described mathematically by means of the double sign operator ‘ \mp ’, with the top sign referring to positive relative rotation of the piers and vice-versa for the bottom one.

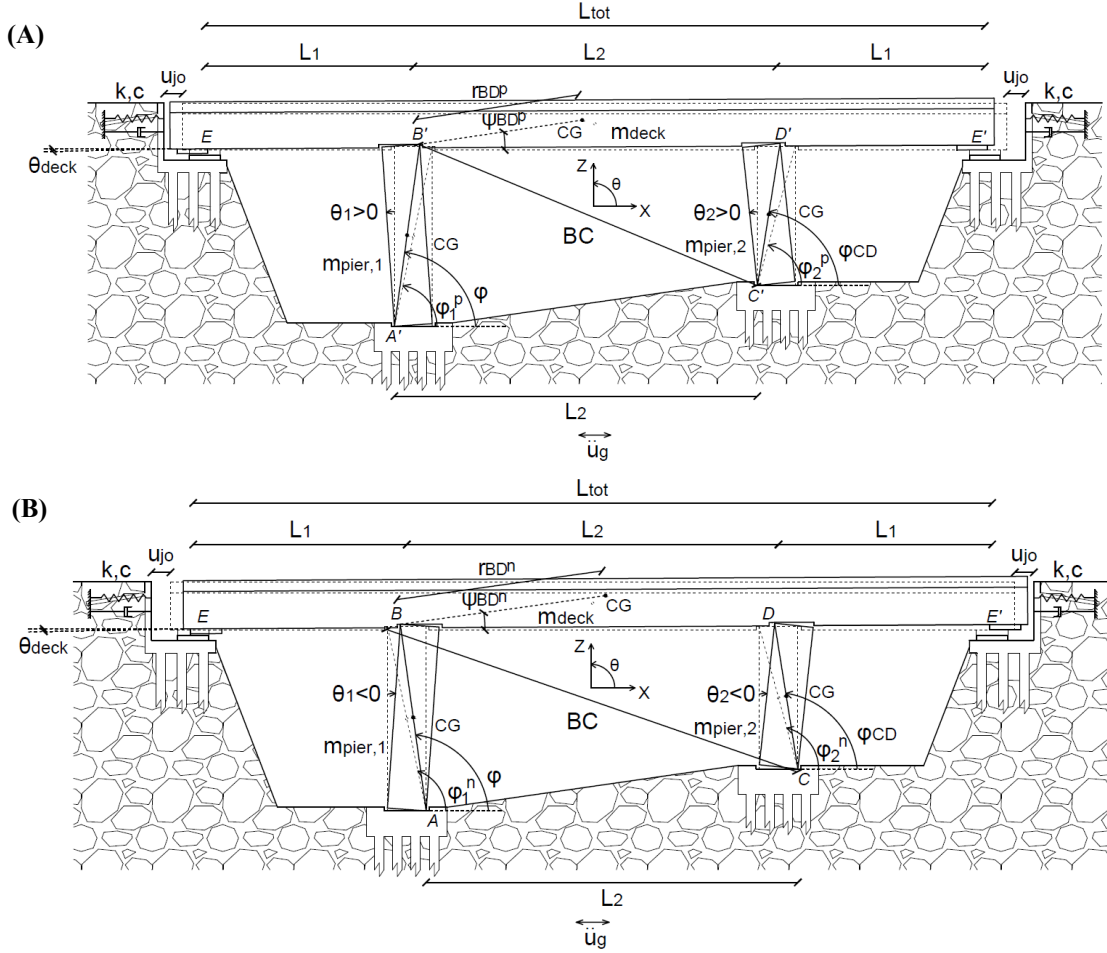


Fig. 2. Schematic of an asymmetric bridge with rocking piers during rocking motion. The structure sustains (A) counter-clockwise (positive) rotation of the piers, and (B) clockwise (negative) rotation of the piers.

Similarly, the rocking rotation of the short pier is $\theta_2 = \varphi_{CD} - \varphi_2^{p/n}$, where $\varphi_2^{p/n} = \pi/2 \mp \alpha_2$ is the angle of this pier at the at-rest rotation. With this notation the dependent variable φ_{CD} is a function of the geometrical properties of the rocking configuration

$$\varphi_{CD} = \pi + \tan^{-1} \left(\frac{R_1 \sin \varphi - r_{AC} \sin \varphi_{AC}}{R_1 \cos \varphi - r_{AC} \cos \varphi_{AC}} \right) - \cos^{-1} \left(\frac{BC^2 + 4R_2^2 - L_2^2}{4R_2 BC} \right), \quad (2)$$

where $BC = \sqrt{(2R_1)^2 + (2r_{AC})^2 - 8R_1 \cdot r_{AC} \cdot \cos(\varphi - \varphi_{AC})}$ is the distance from point B to point C (or from B' to C'), as shown in Fig. 2. Due to the unequal height of the piers, the deck is forced to have a translational movement in the longitudinal and vertical directions (along the X and Z axes, respectively) that occurs simultaneously with its rotational movement (about the Y axis). The rocking rotation of the deck is

$$\theta_{deck} = \tan^{-1} \left(\frac{-R_1 \sin \varphi + r_{AC} \sin \varphi_{AC} + R_2 \sin \varphi_{CD}}{-R_1 \cos \varphi + r_{AC} \cos \varphi_{AC} + R_2 \cos \varphi_{CD}} \right). \quad (3)$$

The longitudinal (u) and the vertical (v) relative displacements of the Centre of Gravity (CG) of the tall and the short piers are expressed in terms of the DoF φ as

$$u_{pier,1}^{CG} = R_1 \cos \varphi \mp B \quad \text{and} \quad v_{pier,1}^{CG} = R_1 \sin \varphi - H_1, \quad (4)$$

$$u_{pier,2}^{CG} = R_2 \cos \varphi_{CD} \mp B \quad \text{and} \quad v_{pier,2}^{CG} = R_2 \sin \varphi_{CD} - H_2, \quad (5)$$

and the corresponding displacements of the CG of the deck are

$$u_{deck}^{CG} = 2R_1 \cos \varphi + r_{BD}^{p/n} \cos(\theta_{deck} + \psi_{BD}^{p/n}) \mp B - \frac{L_2}{2} \quad \text{and} \quad (6)$$

$$v_{deck}^{CG} = 2R_1 \sin \varphi + r_{BD}^{p/n} \sin(\theta_{deck} + \psi_{BD}^{p/n}) - 2H_1 - h,$$

wherein, as shown in Fig. 2, $r_{BD}^{p/n} = \sqrt{h^2 + (L_2/2 \mp B)^2}$ is the length of the segment that connects the upper pivot of the tall pier (B' or B) with the CG of the deck, and $\psi_{BD}^{p/n} = \tan^{-1}(h/(L_2/2 \mp B))$ represents its angle with respect to X. The convention for positive displacements is shown in Fig. 2.

During the free rocking motion of the system, the translational masses of the tall pier ($m_{pier,1} = 8\rho \cdot B^2 \cdot H_1$), of the short pier ($m_{pier,2} = 8\rho \cdot B^2 \cdot H_2$) and of the deck ($m_{deck} = 2\rho \cdot A_{deck} \cdot L_{tot}$) tend to restore the bridge to the at-rest position. Additionally, the rotational masses of all members with respect to the Y axis resist the induced rotational movement according to their corresponding rotational inertias $I_{pier,1}^{CG}$, $I_{pier,2}^{CG}$ and I_{deck}^{CG} .

Initiation of Rocking Motion

The principle of virtual works is applied to the asymmetric bridge at the onset of rocking under a lateral ground acceleration $\ddot{u}_{g,min}$ that is the minimum value capable of inducing uplift in the system

$$m_{pier,1}\ddot{u}_{g,min}\delta u_{pier,1}^{CG} + m_{pier,2}\ddot{u}_{g,min}\delta u_{pier,2}^{CG} + m_{deck}\ddot{u}_{g,min}\delta u_{deck}^{CG} = m_{pier,1}g\delta v_{pier,1}^{CG} + m_{pier,2}g\delta v_{pier,2}^{CG} + m_{deck}g\delta v_{deck}^{CG}, \quad (7)$$

where $\delta u_{pier,1}^{CG}$, $\delta v_{pier,1}^{CG}$, $\delta u_{pier,2}^{CG}$, $\delta v_{pier,2}^{CG}$, δu_{deck}^{CG} and δv_{deck}^{CG} are the partial derivatives of Eqs. (4) to (6) with respect to the DoF of the system, φ . Substituting the relative rotations of the piers (θ_1 and θ_2) into Eq. (7) and by taking into account that the rocking motion initiated at this instant, hence $\theta_1 = \theta_2 = \theta_{deck} = 0$, Eq. (7) is simplified to

$$\ddot{u}_{g,min} = \pm \lambda g \tan \alpha_1 = \pm \frac{m_{pier,1} + m_{pier,2}\bar{h} + m_{deck} \left[1 + \bar{h} - 2\bar{b}(\pm\bar{h} \mp 1) \right]}{m_{pier,1} + m_{pier,2} + 2m_{deck} \left[\frac{\bar{b}h}{H_1}(\pm\bar{h} \mp 1) + 1 \right]} g \tan \alpha_1, \quad (8)$$

where $\bar{h} = H_1/H_2$ is a ratio relating to the level of asymmetry in the height of the piers, and $\bar{b} = B/L_2$. Unlike in the case of symmetric bridges, Eq. (8) shows that for asymmetric bridges the initiation of rocking occurs for different values of the ground acceleration $\ddot{u}_{g,min}$ depending on the direction of motion, while the constant λ is influenced by the geometrical characteristics of the system; it is noted that the latter was found equal to 1 for regular configurations independently of the geometry of the system (Thomaidis *et al.* 2020a). In order to explore the effect of asymmetry through the parameter λ in the value of $\ddot{u}_{g,min}$, Fig. 3 compares the values of $\ddot{u}_{g,min}$ obtained using Eq. (8) for different levels of the pier asymmetry. The bridge considered in the analysis has length $L_{tot} = 2L_1 + L_2 = 2 \cdot 38 + 60 = 136$ m, and the superstructure consists of a simplified single-cell box girder with depth $2h = 1.7$ m, and cross-sectional area $A_{deck} = 6$ m². The bridge has square piers with width $2B = 2.6$ m, height of the tall pier $2H_1 = 26$ m and a height of the short pier $2H_2$ that ranges from 4 m ($\bar{h} = 6.4$) to 26 m ($\bar{h} = 1$) to evaluate the influence of the asymmetry on $\ddot{u}_{g,min}$. The results show that the higher the asymmetry in the height of the rocking piers, the stronger the ground motion should be to initiate rocking motion; the minimum ground acceleration that triggers rocking in the bridge with piers of very unequal height ($\bar{h} = 6.4$, $\ddot{u}_{g,min} = 0.35g$) is 3.5 times larger than the ground acceleration limit for the same bridge with piers of equal height ($\bar{h} = 1$, $\ddot{u}_{g,min} = 0.10g$). We note that the value of λ in Eq. (8) is always greater than 1, and the results included in Fig. 3 indicate that it increases with \bar{h} , particularly for asymmetric bridges with $\bar{h} > 2$. This indicates that designers could potentially delay the initiation or rocking, or even prevent it for moderate earthquakes below certain intensity, if it is possible to reduce the height of the shortest pier while keep the tallest unchanged. Further studies in this direction are recommended in order to propose design recommendations.

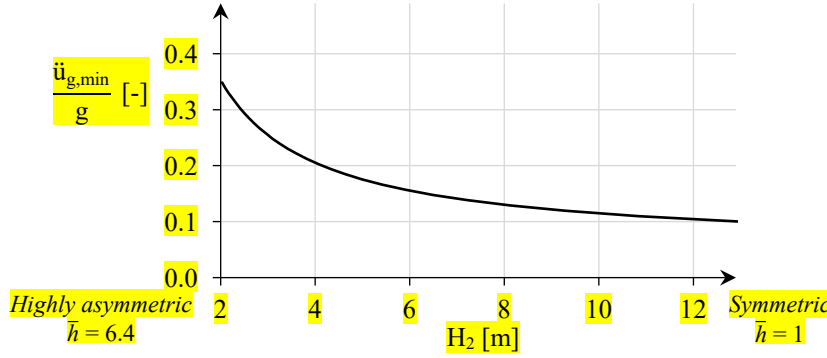


Fig. 3. Minimum ground acceleration to initiate rocking motion ($\ddot{u}_{g,min}$) for bridges with rocking piers of different degree of asymmetry, accounting for the influence of the short pier height (H_2). Results obtained for constant deck mass and cross-section in the tall pier.

It should be noted that Eq. (8) reduces to the rocking initiation acceleration for symmetric bridges given by Thomaidis et al. (2020a) when $\bar{h} = 1$. Moreover, the value of $\ddot{u}_{g,min}$ in asymmetric rocking bridges is identical to that reported by Dimitrakopoulos and Giouvanidis (2015) for asymmetric frames, because the longitudinal and vertical rocking effects at the abutment (neglected in rocking frame models) only appear after rocking starts when the superstructure contacts the abutment backwall and impacts at the abutment seats, respectively (Thomaidis et al. 2020a).

Equation of Motion during Rocking

Considering that the ground motion is strong enough to initiate rocking of the bridge in Fig. 1 (i.e., $\max(|\ddot{u}_g|) > |\ddot{u}_{g,min}|$), its response can be described by the energy balance using Lagrange's equation

$$\frac{d}{dt} \left(\frac{\partial T}{\partial \dot{\phi}} \right) - \frac{\partial T}{\partial \phi} + \frac{\partial V}{\partial \phi} = Q, \quad (9)$$

where T , V and Q are the kinetic energy, the potential energy and the effect of the non-conservative forces, respectively. The kinetic energy of the system with respect to the corresponding CG of the members is

$$T = \frac{1}{2} m_{pier,1} [\dot{u}_{pier,1}^{CG^2} + \dot{v}_{pier,1}^{CG^2}] + \frac{1}{2} I_{pier,1}^{CG} \dot{\phi}^2 + \frac{1}{2} m_{pier,2} [\dot{u}_{pier,2}^{CG^2} + \dot{v}_{pier,2}^{CG^2}] + \frac{1}{2} I_{pier,2}^{CG} \dot{\phi}_{CD}^2 + \frac{1}{2} m_{deck} [\dot{u}_{deck}^{CG^2} + \dot{v}_{deck}^{CG^2}] + \frac{1}{2} I_{deck}^{CG} \dot{\theta}_{deck}^2, \quad (10)$$

where $\dot{u}_{pier,1}^{CG}$, $\dot{v}_{pier,1}^{CG}$, $\dot{u}_{pier,2}^{CG}$, $\dot{v}_{pier,2}^{CG}$, \dot{u}_{deck}^{CG} and \dot{v}_{deck}^{CG} are the first time-derivatives of Eqs. (4) to (6), respectively, while the angular velocities of the short pier ($\dot{\phi}_{CD} = \dot{\theta}_2$) and the deck ($\dot{\theta}_{deck}$) are

$$\dot{\phi}_{CD} = \frac{d\phi_{CD}}{dt} = \frac{\partial \phi_{CD}}{\partial \phi} \frac{d\phi}{dt} = \frac{\partial \phi_{CD}}{\partial \phi} \dot{\phi}, \quad (11)$$

$$\dot{\theta}_{deck} = \frac{d\theta_{deck}}{dt} = \frac{\partial \theta_{deck}}{\partial \phi} \frac{d\phi}{dt} = \frac{\partial \theta_{deck}}{\partial \phi} \dot{\phi}. \quad (12)$$

By introducing Eqs. (11) and (12) into Eq. (10), the total kinetic energy of the system with respect to the active pivot point (as explained below) of each member is

$$T = \left[\frac{1}{2} I_{pier,1}^{Pivot} + \frac{1}{2} I_{pier,2}^{Pivot} \left(\frac{\partial \phi_{CD}}{\partial \phi} \right)^2 + \frac{1}{2} I_{deck}^{Pivot} \left(\frac{\partial \theta_{deck}}{\partial \phi} \right)^2 + m_{deck} \left(2R_1^2 + 2R_1 r_{BD}^{p/n} \cos(\phi - \theta_{deck} - \psi_{BD}^{p/n}) \frac{\partial \theta_{deck}}{\partial \phi} \right) \right] \dot{\phi}^2, \quad (13)$$

wherein $I_{pier,i}^{Pivot} = 4m_{pier,i} \cdot R_i^2/3$ is the mass moment of inertia of the i -th pier with respect to one of its bottom corners (pivot point) that drive the rocking motion, with $i = 1, 2$; $I_{deck}^{Pivot} = I_{deck}^{CG} + m_{deck} \cdot r_{BD}^{p/n \cdot 2}$ is the mass moment of inertia of the deck with respect to the active pivot points at the deck-pier contacts.

The potential energy components that describe the gravity effects (V_{in}) and the elastic spring forces at the abutments (V_{as}) are

$$V_{in} = g \left[m_{pier,1} v_{pier,1}^{CG} + m_{pier,2} v_{pier,2}^{CG} + m_{deck} v_{deck}^{CG} \right], \quad (14)$$

$$V_{as} = \begin{cases} 0 \\ \frac{1}{2} k \left[u_{deck}^{CG} \pm u_{jo} \right]^2 \end{cases} \quad \text{if} \quad \begin{cases} |u_{deck}^{CG}| < u_{jo} \\ |u_{deck}^{CG}| \geq u_{jo} \end{cases}. \quad (15)$$

The total potential energy of the free-standing asymmetric system is $V = V_{in} + V_{as}$. It can be obtained by introducing Eqs. (4) to (6) in Eqs. (14) and (15), but it is not included here, for economy of space.

The total effect of the generalized forces is $Q = Q_{in} + Q_{ad}$, with $Q_{in} = \partial W_{in} / \partial \phi$ and $Q_{ad} = \partial W_{ad} / \partial \phi$ given by the variation of the virtual work $\delta W_{in} = -\ddot{u}_g \cdot [m_{pier,1} \cdot u_{pier,1}^{CG} + m_{pier,2} \cdot u_{pier,2}^{CG} + m_{deck} \cdot u_{deck}^{CG}]$ and $\delta W_{ad} = -c \cdot \dot{u}_{deck}^{CG} \cdot [u_{deck}^{CG} \pm u_{jo}]$, respectively. Substituting Eqs. (4) to (6) and the first time-derivative of Eq. (6) in the expressions of the generalized forces

$$Q_{in} = \ddot{u}_g \left[\begin{aligned} & \left(m_{pier,1} + 2m_{deck} \right) R_1 \sin \varphi + m_{pier,2} R_2 \sin \varphi_{CD} \frac{\partial \varphi_{CD}}{\partial \varphi} \\ & + m_{deck} r_{BD}^{p/n} \sin \left(\theta_{deck} + \psi_{BD}^{p/n} \right) \frac{\partial \theta_{deck}}{\partial \varphi} \end{aligned} \right], \quad (16)$$

$$Q_{ad} = -4cR_1^2 \left[\sin \varphi + \bar{r}^{p/n} \sin \left(\theta_{deck} + \psi_{BD}^{p/n} \right) \frac{\partial \theta_{deck}}{\partial \varphi} \right]^2 \dot{\varphi}, \quad (17)$$

in which $\bar{r}^{p/n} = r_{BD}^{p/n} / 2R_1$.

Introducing Eqs. (13) - (17) into Eq. (9) yields the EoM for the asymmetric rocking bridge

$$\ddot{\varphi} = -\frac{g}{R_1} \left[\overbrace{-\frac{R_1}{g} \left(\frac{T_{f2}(\varphi)}{T_{f1}(\varphi)} \right) \dot{\varphi}^2 + \left(\frac{V_{inf}(\varphi)}{T_{f1}(\varphi)} \right) - \frac{\ddot{u}_g}{g} \left(\frac{Q_{inf}(\varphi)}{T_{f1}(\varphi)} \right)}^{\text{frame system}} \right] - \overbrace{\frac{g}{R_1} q \left[k \left(\frac{V_{asf}(\varphi)}{T_{f1}(\varphi)} \right) + c \left(\frac{Q_{adf}(\varphi)}{T_{f1}(\varphi)} \right) \dot{\varphi} \right]}^{\text{abutment-backfill contribution}}, \quad (18)$$

where

$$\begin{aligned} T_{f1}(\varphi) &= \frac{I_{pier,1}^{Pivot}}{R_1^2} + \frac{I_{pier,2}^{Pivot}}{R_1^2} \left(\frac{\partial \varphi_{CD}}{\partial \varphi} \right)^2 + m_{deck} \left[4 + 8\bar{r}^{p/n} \cos \left(\varphi - \theta_{deck} - \psi_{BD}^{p/n} \right) \frac{\partial \theta_{deck}}{\partial \varphi} \right] + \frac{I_{deck}^{Pivot}}{R_1^2} \left(\frac{\partial \theta_{deck}}{\partial \varphi} \right)^2 \\ T_{f2}(\varphi) &= \frac{I_{pier,2}^{Pivot}}{R_1^2} \frac{\partial \varphi_{CD}}{\partial \varphi} \frac{\partial^2 \varphi_{CD}}{\partial \varphi^2} + 4m_{deck} \bar{r}^{p/n} \left[\cos \left(\varphi - \theta_{deck} - \psi_{BD}^{p/n} \right) \frac{\partial^2 \theta_{deck}}{\partial \varphi^2} \right. \\ &\quad \left. - \sin \left(\varphi - \theta_{deck} - \psi_{BD}^{p/n} \right) \frac{\partial \theta_{deck}}{\partial \varphi} \left(1 - \frac{\partial \theta_{deck}}{\partial \varphi} \right) \right] \\ &\quad + \frac{I_{deck}^{Pivot}}{R_1^2} \frac{\partial \theta_{deck}}{\partial \varphi} \frac{\partial^2 \theta_{deck}}{\partial \varphi^2} \end{aligned}$$

$$V_{inf}(\varphi) = \left[m_{pier,1} + 2m_{deck} \right] \cos \varphi + m_{pier,2} \bar{R} \cos \varphi_{CD} \frac{\partial \varphi_{CD}}{\partial \varphi} + 2m_{deck} \bar{r}^{p/n} \cos \left(\theta_{deck} + \psi_{BD}^{p/n} \right) \frac{\partial \theta_{deck}}{\partial \varphi}$$

$$Q_{inf}(\varphi) = \left[m_{pier,1} + 2m_{deck} \right] \sin \varphi + m_{pier,2} \bar{R} \sin \varphi_{CD} \frac{\partial \varphi_{CD}}{\partial \varphi} + 2m_{deck} \bar{r}^{p/n} \sin \left(\theta_{deck} + \psi_{BD}^{p/n} \right) \frac{\partial \theta_{deck}}{\partial \varphi}$$

$$\begin{aligned}
206 \quad V_{asf}(\varphi) &= \left[m_{pier,1} + m_{pier,2} + 3m_{deck} \right] \left[\begin{aligned} & -\cos \varphi - \bar{r}^{p/n} \cos(\theta_{deck} + \psi_{BD}^{p/n}) \\ & \pm \frac{B}{2R_1} + \frac{L_2}{4R_1} \mp \frac{u_{jo}}{2R_1} \end{aligned} \right] \\
207 \quad & \left[\sin \varphi + \bar{r}^{p/n} \sin(\theta_{deck} + \psi_{BD}^{p/n}) \frac{\partial \theta_{deck}}{\partial \varphi} \right] \\
208 \quad Q_{adf}(\varphi) &= \left[m_{pier,1} + m_{pier,2} + 3m_{deck} \right] \left[\sin \varphi + \bar{r}^{p/n} \sin(\theta_{deck} + \psi_{BD}^{p/n}) \frac{\partial \theta_{deck}}{\partial \varphi} \right],
\end{aligned}$$

209 and $\bar{R} = R_2/R_1$. The EoM described in Eq. (18) is composed of two parts; the first one (*'frame system'*) describes the
210 motion before the deck contacts the abutments in the longitudinal direction ($|u_{deck}^{CG}| < u_{jo}$), whilst the second term
211 (*'abutment-backfill contribution'*) is only active when the deck contacts the abutments longitudinally ($|u_{deck}^{CG}| \geq u_{jo}$),
212 and it describes the constraint of the rocking motion of the frame due to the presence of the abutment-backfill system.
213 This second term has a significant effect on the seismic response of asymmetric rocking bridges, as shown below. If
214 there is no contact between the superstructure and the abutments at the ends of the deck ($|u_{deck}^{CG}| < u_{jo}$), the spring
215 stiffness (k) and the dashpot coefficient (c) of the end supports are neglected and the EoM reduces to that of an
216 asymmetric frame without end restraints as presented by Dimitrakopoulos and Giouvanidis (2015). Moreover, Eq.
217 (18) coincides with the corresponding EoM for symmetric bridges presented by Thomaidis et al. (2020a) for the case
218 of two rocking piers with same height ($\bar{h} = 1$ and $m_{pier,1} = m_{pier,2}$). In this context, the proposed EoM is a generalization
219 of the aforementioned works.

220 The effect of the abutment-backfill system on the longitudinal rocking response is directly linked to the
221 parameter $q = 4R_1/g \cdot [m_{pier,1} + m_{pier,2} + 3m_{deck}]$, and it is beneficial as $q > 1$. In order to explore this effect, we
222 consider a typical bridge with square piers of dimension $2B = 2.6$ m and height of the tall pier $2H_1 = 26$ m, thus
223 resulting in $m_{pier,1} = 44 \cdot 10^4$ kg, and a deck mass $m_{deck} = 200 \cdot 10^4$ kg. Fig. 4 plots the value of q with respect to the
224 mass of the short pier ($m_{pier,2}$), which is obtained by changing the height of this member ($2H_2$) from 26 m (symmetric
225 case, $\bar{h} = 1$) to 5.2 m (asymmetric case, $\bar{h} = 5$). It is seen from Fig. 4 that bridges in which the mass of the short pier
226 is much smaller than that of the long one (i.e., with a higher level of asymmetry), have larger interaction with the
227 abutment-backfill system due to the reduction in the total mass of the system. However, the difference between the
228 two extreme cases is only 4%, which shows that the contribution of the abutment-backfill system is not significantly
229 affected by differences in the height of the piers.

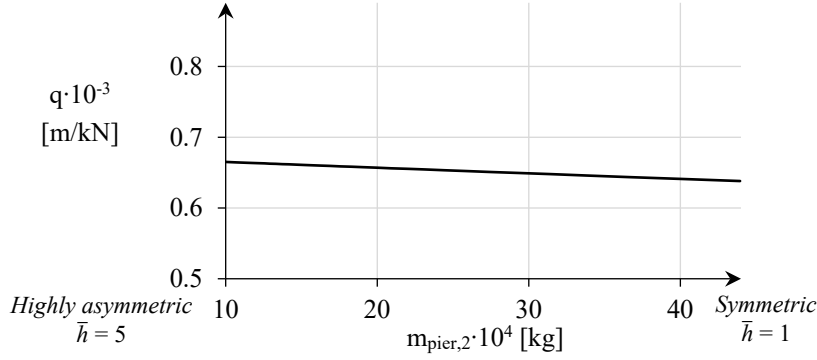


Fig. 4. Influence of the abutment-backfill system (q) in bridges with rocking piers of different degree of asymmetry expressed by the mass of the short pier ($m_{pier,2}$). Results obtained when the tall pier section and the deck mass are constant.

Impact on the Abutment Backwall

When a bridge starts rocking as described by Eq. (8), the term of the EoM in Eq. (18) that is related to the ‘*frame system*’ describes the time-history of the angle of rotation (φ) of the tall pier before the deck is in contact with the abutments. If the joint gap is closed ($|u_{deck}^{CG}| = u_{jo}$), the deck impacts on the backwall of one of the abutments. This impact dissipates energy instantly, and subsequently the structure either behaves as a frame system in a free rocking motion described by the first part of Eq. (18) (i.e., ‘*frame system*’) if the dissipation is large enough and the ground motion decays, or otherwise it continues activating the abutment-backfill system and the time-history of angle of rotation is described by both parts of Eq. (18) (i.e., ‘*frame system*’ plus ‘*abutment-backfill contribution*’).

The pounding problem is modelled using several concepts (e.g., Muthukumar and DesRoches 2006, Shi and Dimitrakopoulos 2017), the key idea being to capture the attenuation of motion whenever an impact between superstructure and abutment takes place. The present study adopts the ‘*stereomechanical approach*’ based on the conservation of linear momentum in the normal direction, as described in the study of Muthukumar and DesRoches (2006). This approach utilizes the CoR (e) to describe pounding. Fig. 5A illustrates the superstructure of the rocking system just before impacting on the abutment backwall with a longitudinal velocity $\dot{u}_{deck,I}^{CG}$, while Fig. 5B depicts the post-pounding condition where the superstructure moves longitudinally, either towards the at-rest position or towards the abutment-backfill system, with a decreased value of longitudinal velocity $\dot{u}_{deck,II}^{CG}$.

The pre-pounding and post-pounding longitudinal velocities of the superstructure are related as follows

$$\dot{u}_{deck,II}^{CG} = \dot{u}_{deck,I}^{CG} - [1 + e] \frac{m_{abut.} [\dot{u}_{deck,I}^{CG}]}{m_{abut.} + m_{deck}}, \quad (19)$$

wherein $m_{abut.} = \rho_s \cdot L_{cr.} \cdot B_{abut.} \cdot h_{bw}$ refers to the mass of the backfill related to the mass density of the soil (ρ_s), the length of the backfill soil that is expected to resist the impact of the superstructure on the abutment backwall ($L_{cr.}$), as well as the width ($B_{abut.}$) and the height (h_{bw}) of the abutment backwall that represent the contact surface between the deck and the abutment. It is noted that this definition of $m_{abut.}$ is valid for seat-type abutments with ‘sacrificial’ backwalls; when this is not the case, a larger mass of the abutment will resist the deck impact (through passive pressure), and in that case the proposed value is on the safe side. Introducing the first time-derivative of Eq. (6) in Eq. (19) gives the ratio of the angular velocities of the tall pier ($\dot{\phi}_{II}/\dot{\phi}_I$) to describe the pounding effect in the abutments of asymmetric bridges with rocking piers

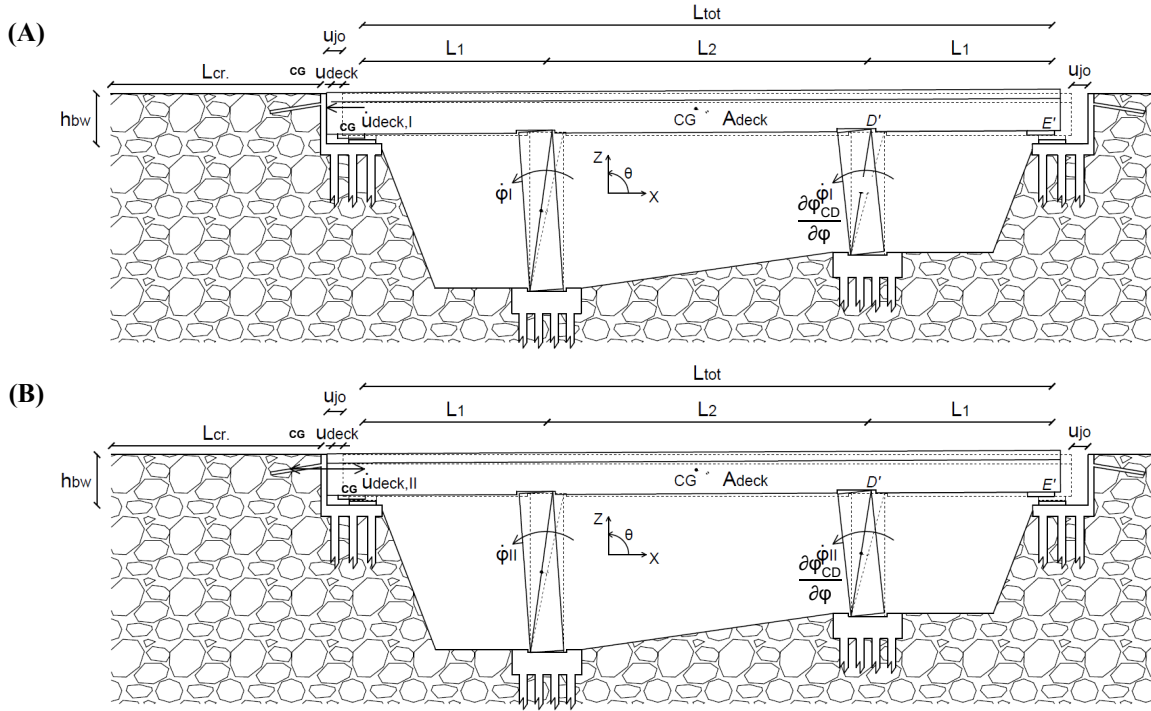


Fig. 5. Schematic of the pounding problem considered in the rocking motion of an asymmetric bridge with rocking piers, including (A) the pre-pounding state with a longitudinal velocity of the superstructure $\dot{u}_{deck,I}^{CG}$, and (B) the post-pounding state with an associated deck velocity $\dot{u}_{deck,II}^{CG}$.

$$\frac{\dot{\phi}_{II}^{CG}}{\dot{\phi}_I^{CG}} = \frac{\dot{\phi}_{II}}{\dot{\phi}_I} = 1 - [1 + e] \frac{m_{abut.}}{m_{abut.} + m_{deck}} \quad (20)$$

Thus, when the superstructure impacts on the abutments, the angular velocity of the tall pier will be reduced according to Eq. (20).

Impact at the Rocking Interfaces

During the rocking motion, when the structure returns to the at-rest position ($\theta_1 = \theta_2 = \theta_{deck} = 0$ or $\varphi = \varphi_1^{p/n}$) impacts at the rocking interfaces occur, thus dissipating energy. This is described by means of a CoR $\eta = |\dot{\varphi}_{II}/\dot{\varphi}_I|$ that relates the independent variable of the angular velocity of the tall pier before and after impact ($\dot{\varphi}_I$, and $\dot{\varphi}_{II}$, respectively). An impulse formulation is adopted here that extends the work of Dimitrakopoulos and Giouvanidis (2015) by incorporating in the formulation the effect of the abutments acting as vertical supports, as well as the length of the end spans (L_1). This is based on the following assumptions:

- The reversal of the rocking direction at each impact at the rocking interfaces takes place smoothly, without bouncing or sliding. Therefore, the angular momentum is conserved just before and after the impact. This is strictly valid only for slender piers (Cheng 2007) and for large values of the coefficient of friction (Di Egidio and Contento 2009).
- The impact forces are concentrated at the corresponding pivot points (Housner 1963), thus ignoring the potential migration of the resultant force towards the center of the pier base due to an extended contact surface (Kalliontzis et al. 2016).

and these assumptions have been found accurate in the study of Bachmann *et al.* (2018) who showed that the analytical model of Housner (1963) is capable of capturing experimental results in a statistical sense.

Without loss of generality, let the displaced position of the bridge change from counter-clockwise (positive) to clockwise (negative) as shown in Fig. 6. Considering that additional reaction forces (or impulses) are developed at the abutment seats compared to the corresponding asymmetric frame without abutments, there are seven unknowns that need to be determined. These are the impulses $\Lambda_{A,x}$ and $\Lambda_{A,z}$ at pivot A of the tall pier, $\Lambda_{C,x}$ and $\Lambda_{C,z}$ at pivot C of the short pier, $\Lambda_{E,z}$ as well as $\Lambda_{E',z}$ at the two abutment seats E and E', respectively, and the angular velocity of the tall pier after the impact at the rocking interfaces $\dot{\varphi}_{II}$. However, only five equations can be used to describe the impact problem. For this reason, two additional relationships between the impulses at the abutment seats and those at the pier-deck interfaces are introduced, based on the fraction of the weight of the deck that is resisted by each support of the bridge under gravity loading

$$\Lambda_{E,z} = \frac{L_1}{L_1 + L_2} \Lambda_{B,z}, \quad (21)$$

$$\Lambda_{E',z} = \frac{L_1}{L_1 + L_2} \Lambda_{D,z}. \quad (22)$$

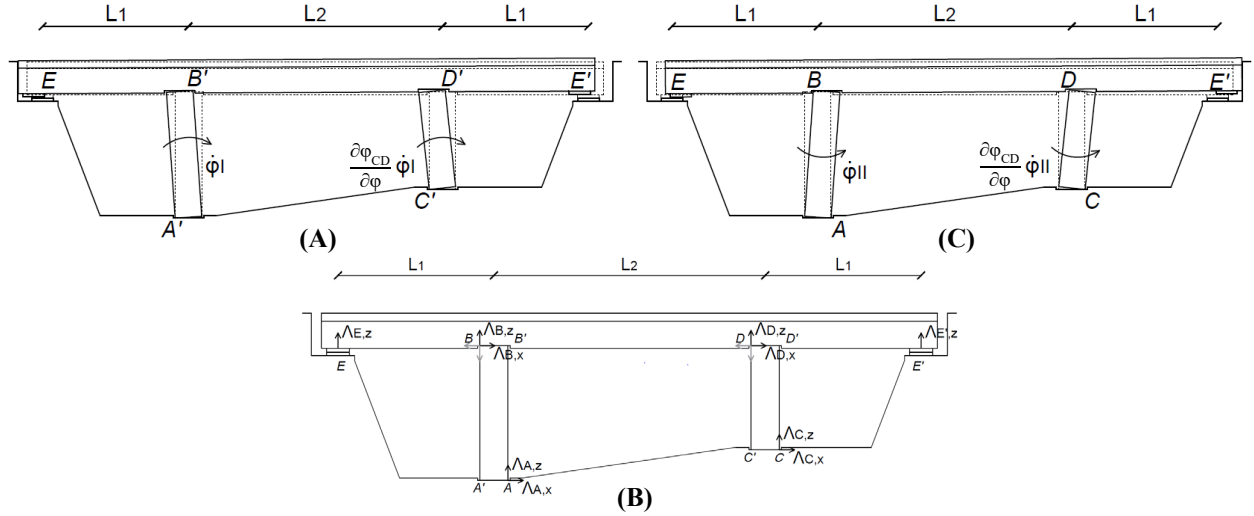


Fig. 6. Schematic of the impact problem considered in the rocking motion of an asymmetric bridge with rocking piers that (A) undergoes counter-clockwise (positive) rotation with an angular velocity of the tall pier $\dot{\phi}_I$, (B) impacts at the corresponding pivot points, and then reverses to (C) clockwise (negative) rotation with an angular velocity of the tall pier $\dot{\phi}_{II}$.

Introducing the conservation of linear momentum before and after impact at the rocking interfaces along the Z axis for the tall and the short piers into Eqs. (21) and (22), respectively, establishes the relationship between the impacts at the abutments (E-E') and those at the base of the piers (A-C)

$$\Lambda_{E,z} = \frac{L_1}{L_1 + L_2} \left[\Lambda_{A,z} + m_{pier,1} B (\dot{\phi}_I + \dot{\phi}_{II}) \right]. \quad (23)$$

$$\Lambda_{E',z} = \frac{L_1}{L_1 + L_2} \left[\Lambda_{C,z} + m_{pier,2} B \bar{h} (\dot{\phi}_I + \dot{\phi}_{II}) \right]. \quad (24)$$

Eqs. (23) and (24) reduce the unknowns of the impact problem from seven to five ($\Lambda_{A,x}$, $\Lambda_{A,z}$, $\Lambda_{C,x}$, $\Lambda_{C,z}$ and $\dot{\phi}_{II}$), and the following equations are considered in the determination of these unknowns;

1. Linear momentum along the longitudinal (X) axis for the entire bridge

$$\Lambda_{A,x} + \Lambda_{C,x} = \left[m_{pier,1} + m_{pier,2} + 2m_{deck} \right] H_1 (\dot{\phi}_I - \dot{\phi}_{II}) + 2m_{deck} \bar{b} h \left[\bar{h} - 1 \right] (\dot{\phi}_I + \dot{\phi}_{II}). \quad (25)$$

2. Linear momentum along the vertical (Z) axis for the entire bridge

$$\begin{aligned}
& \Lambda_{E,z} + \Lambda_{A,z} + \Lambda_{C,z} + \Lambda_{E',z} = \\
& 2m_{deck}B\bar{b}\left[\bar{h}-1\right](\dot{\phi}_I - \dot{\phi}_{II}) - \left[m_{pier,1}B + m_{pier,2}B\bar{h} + m_{deck}B(\bar{h}+1)\right](\dot{\phi}_I + \dot{\phi}_{II}).
\end{aligned} \tag{26}$$

3. Angular momentum about pivot B for the tall pier

$$2H_1\Lambda_{A,x} + 2B\Lambda_{A,z} = \left[m_{pier,1}H_1^2 - I_{pier,1}^{CG}\right](\dot{\phi}_I - \dot{\phi}_{II}) - m_{pier,1}B^2(\dot{\phi}_I + \dot{\phi}_{II}). \tag{27}$$

4. Angular momentum about pivot D for the short pier

$$2H_2\Lambda_{C,x} + 2B\Lambda_{C,z} = \left[m_{pier,2}H_1H_2 - I_{pier,2}^{CG}\bar{h}\right](\dot{\phi}_I - \dot{\phi}_{II}) - m_{pier,2}B^2\bar{h}(\dot{\phi}_I + \dot{\phi}_{II}). \tag{28}$$

5. Angular momentum about pivot A for the entire bridge

$$\begin{aligned}
& -[L_1 + B]\Lambda_{E,z} - [2H_1 - 2H_2]\Lambda_{C,x} \\
& + L_2\Lambda_{C,z} + [L_1 + L_2 - B]\Lambda_{E',z} = \\
& \left[-m_{pier,1}H_1^2 - I_{pier,1}^{CG} - m_{pier,2}H_1(2H_1 - H_2) - I_{pier,2}^{CG}\bar{h} \right] (\dot{\phi}_I - \dot{\phi}_{II}) \\
& - 2m_{deck}H_1(2H_1 + h) + 2m_{deck}\left(\frac{L_2}{2} - B\right)B\bar{b}(\bar{h} - 1) \Bigg] (\dot{\phi}_I - \dot{\phi}_{II}) \\
& + \left[m_{pier,1}B^2 - m_{pier,2}B\bar{h}(L_2 - B) - 2m_{deck}(2H_1 + h)\bar{b}h(\bar{h} - 1) \right] (\dot{\phi}_I + \dot{\phi}_{II}) \\
& - m_{deck}\left(\frac{L_2}{2} - B\right)B(\bar{h} + 1) - I_{deck}^{CG}2\bar{b}(\bar{h} - 1) \Bigg] (\dot{\phi}_I + \dot{\phi}_{II})
\end{aligned} \tag{29}$$

After solving the system of equations, the CoR at the rocking interfaces $\eta = |\dot{\phi}_{II}/\dot{\phi}_I|$ is given by

$$\begin{aligned}
& \alpha_1[H_1^2 - B^2]m_{pier,1} + \alpha_1 I_{pier,1}^{CG} + \alpha_1[H_1^2 - \bar{h}^2 B^2]m_{pier,2} + \alpha_1 \bar{h}^2 I_{pier,2}^{CG} \\
& + \left[4\alpha_1 H_1^2 \pm 4\alpha_2 H_1 h \bar{b}(\bar{h} - 1) - 4\alpha_3 h^2 \bar{b}^2(\bar{h} - 1)^2 \right. \\
& \left. - B^2\left(\alpha_4(\bar{h} + 1)^2 - 4\alpha_5 \bar{b}^2(\bar{h} - 1)^2\right) \mp 2\alpha_6 \bar{b}(\bar{h}^2 - 1) \right] m_{deck} \\
& - 4\alpha_3 \bar{b}^2[\bar{h} - 1]^2 I_{deck}^{CG} \\
& \eta^{p/n} = \left| \frac{\dot{\phi}_{II}}{\dot{\phi}_I} \right| = \frac{ }{ \alpha_1[H_1^2 + B^2]m_{pier,1} + \alpha_1 I_{pier,1}^{CG} + \alpha_1[H_1^2 + \bar{h}^2 B^2]m_{pier,2} + \alpha_1 \bar{h}^2 I_{pier,2}^{CG} } \\
& + \left[4\alpha_1 H_1^2 \mp 4\alpha_7 H_1 h \bar{b}(\bar{h} - 1) + 4\alpha_3 h^2 \bar{b}^2(\bar{h} - 1)^2 \right. \\
& \left. + B^2\left(\alpha_4(\bar{h} + 1)^2 + 4\alpha_5 \bar{b}^2(\bar{h} - 1)^2\right) \pm 2\alpha_8 \bar{b}(\bar{h}^2 - 1) \right] m_{deck} \\
& + 4\alpha_3 \bar{b}^2[\bar{h} - 1]^2 I_{deck}^{CG}
\end{aligned} \tag{30}$$

where

$$\begin{aligned}
 \alpha_1 &= 4\bar{L}^3 + 6\bar{L}^2 + 4\bar{L} + 1 & \alpha_2 &= 4\bar{L}^3 + 4\bar{L}^2 + \bar{L} & \alpha_3 &= 2\bar{L}^2 + 3\bar{L} + 1 \\
 \alpha_4 &= 2\bar{L}^3 + 4\bar{L}^2 + 3\bar{L} + 1 & \alpha_5 &= [\bar{L} + 1]^2 & \alpha_6 &= 2\bar{L}^3 + 3\bar{L}^2 + \bar{L} \\
 \alpha_7 &= 4\bar{L}^3 + 8\bar{L}^2 + 7\bar{L} + 2 & \alpha_8 &= 2\bar{L}^3 + 5\bar{L}^2 + 5\bar{L} + 2
 \end{aligned}$$

and $\bar{L} = L_1/L_2$ describes the effect of the span arrangement. It is observed that, due to the asymmetric configuration, Eq. (30) depends on the direction of rocking reversal, and the value of η obtained with the upper signs in the operators ‘ \pm ’ and ‘ \mp ’ corresponds to the movement in which the rotation of the rocking piers changes from positive to negative, and vice-versa for the lower signs; the impulse formulation that leads to the bottom signs of Eq. (30) is not presented herein (for brevity), and can be found in Thomaidis (2020). It must be noted that both expressions of Eq. (30) (i.e., with upper or lower signs) reduce to the CoR at the rocking interfaces of the symmetric bridges with two rocking piers (Thomaidis et al. 2020a) when both piers have the same height.

Eq. (30) is different from that for the CoR η in asymmetric frames with rocking columns (Dimitrakopoulos and Giouvanidis 2015) due to the additional impulses developed at the abutment seats. If such impulses are neglected ($\Lambda_{E,z} = \Lambda_{E',z} = 0$) in the system of Eqs. (25) to (29), the solution of this system of equations gives exactly the CoR derived by Dimitrakopoulos and Giouvanidis (2015) for asymmetric frames. To this end, and to establish the effect of the additional impacts at the end of the superstructure in the value of η , Fig. 7 compares the values obtained using Eq. (30) with those from the corresponding expression for asymmetric rocking frames. The bridge considered in this comparison has three spans of equal length ($\bar{L} = 1$), to make the expression proposed by Dimitrakopoulos and Giouvanidis (2015) applicable. The bridge has square piers with width $2B = 2.5$ m, height of the tall pier $2H_1 = 30$ m and a height of the short pier $2H_2$ that ranges from 6 m ($\bar{h} = 5$) to 30 m ($\bar{h} = 1$) to evaluate the influence of the asymmetry on the response. The superstructure in the bridges and frames has length $L_{tot} = 2L_1 + L_2 = 2 \cdot 45 + 45 = 135$ m and consists in a simplified single-cell box girder with depth $2h = 2$ m, width of the bottom and the top slabs $B_{bot} = 6.5$ m and $B_{top} = 10$ m, respectively, and flange and wall thicknesses $t_f = 0.35$ m and $t_w = 0.9$ m, respectively, thus resulting in $A_{deck} = 7$ m². The mass of the tall pier is equal to $m_{pier,1} = 47 \cdot 10^4$ kg and that of the superstructure is $m_{deck} = 240 \cdot 10^4$ kg, while the mass moment of inertia of the box girder section of the deck is $I_{deck}^{CG} = 360 \cdot 10^7$ kg·m². The results show that the value of η is always larger in the bridge than in the corresponding frame with the same dimensions. This indicates that the presence of the abutment (vertical) supports reduces the energy dissipation (at the

pier-deck interfaces) as the abutments carry part of the deck weight. The increase in the value of η for bridges with rocking piers with respect to the equivalent frames is relatively small for levels of asymmetry below $\bar{h} = 2$ (the difference is 0.5% for the symmetric configuration, $\bar{h} = 1$), but it increases significantly above this value, reaching 12.5% for the highly asymmetric configuration ($\bar{h} = 5$). This is expected taking into account that the effect of the deck weight carried by the piers due to the presence of the end supports is more significant when short piers are considered (i.e., as in highly asymmetric configurations) noting that in the case of tall piers the total weight impacting on the bottom rocking interfaces is already large due to the self-weight of the pier.

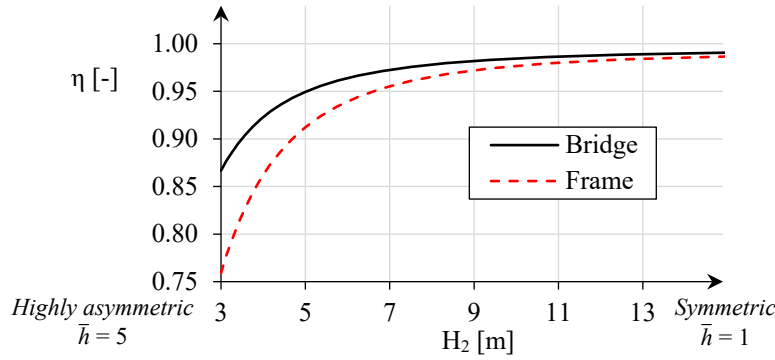


Fig. 7. CoR at the rocking interfaces (η) for bridges with rocking piers of different degree of asymmetry and for corresponding frames (Dimitrakopoulos and Giouvanidis 2015), accounting for the influence of the short pier height (H_2). Results obtained for constant deck mass and tall pier section.

The value of the CoR at the rocking interfaces of the asymmetric bridge described in Eq. (30) is also influenced by the span arrangement (lengths L_1 and L_2). The effect of these parameters on η is presented in Fig. 8, which considers the same bridge dimensions as in the previous study on the influence of the pier asymmetry, with the exception of a constant height of the short pier equal to $2H_2 = 20$ m ($\bar{h} = 1.5$) and variable span lengths. For comparison purposes, the mass of the deck is kept constant ($m_{deck} = 240 \cdot 10^4$ kg), regardless of its length. It is seen from Fig. 8A (depicting influence of L_1 for constant $L_2 = 45$ m) that by increasing the length of the end spans (L_1) while keeping constant the length of the intermediate spans (L_2) the CoR η increases slightly, leading to lower energy dissipation. This is due to the axial forces at the piers that are progressively decreasing (they are increasing at the abutment seats), which reduces the energy dissipation at every impact at the rocking interfaces during the rocking motion. On the other hand, Fig. 8B (depicting influence of L_2 for constant $L_1 = 45$ m) shows that higher amount of energy is dissipated when the length of the central span (L_2) is increased while keeping constant the length of the end spans (L_1); the justification is based on the same reasoning as before.

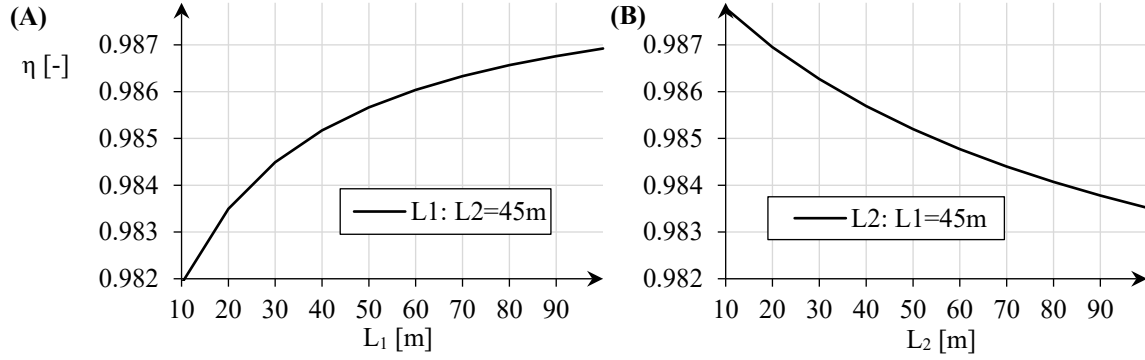


Fig. 8. CoR at the rocking interfaces (η) for asymmetric bridges with rocking piers, accounting for the influence of (A) the length of the end spans (L_1) and (B) the length of the intermediate spans (L_2). Results obtained for constant deck mass.

It must be noted that the CoR calculated from Eq. (30) and presented in Figs. 7 and 8 is conservative, i.e. higher than those expected in reality because the analytical formulation ignores (i) the angular velocity just before impact (Jankowski 2007), (ii) the inelastic behaviour of the interface material at the instant of impact (Roh and Reinhorn 2010), (iii) the sliding effects that take place during rocking motion (Chatzis and Smyth 2012b) and (iv) the imperfections of the contact surfaces (ElGawady et al. 2011).

RESPONSE HISTORY ANALYSIS OF ASYMMETRIC ROCKING BRIDGES UNDER GROUND MOTIONS

This section addresses the seismic response of symmetric ($\bar{h} = 1$) and asymmetric ($\bar{h} > 1$) bridges with rocking piers subjected to seismic ground motions. The rocking motion is analyzed using an algorithm based on the equations given in the previous section, implemented in MATLAB (2016). The analysis starts with the calculation of the minimum ground acceleration that initiates rocking using Eq. (8). If the ground motion is not capable of exceeding this value, rocking motion does not take place and the piers remain in a vertical position. When this is not the case, the EoM Eq. (18) is integrated step-by-step using the Runge-Kutta method with a time-step of 10^{-3} s that was selected through a sensitivity analysis. Response-history analysis of bridges with rocking piers requires identifying the instants at which impact on the abutment backwall ($|u_{deck}^{CG}| = u_{jo}$), and at the rocking interfaces ($\varphi = \varphi_1^{p/n}$) occur. This is implemented in the code with an iterative process that reduces the time-step down to a value of $5 \cdot 10^{-6}$ s in the vicinity of these impact effects. After impact is identified, the next time-step updates the angular velocity of the rocking motion using the restitution coefficients defined in Eqs. (20) and (30). Failure of the rocking structures, as defined in the following, is checked at each time-step of the analysis and triggers its termination if met.

For practical implementation, a simplified procedure was devised for analyzing asymmetric bridges governed by EoM Eq. (18). The procedure aimed to avoid using the full expressions for the first and second partial derivatives of Eq. (2) with respect to the DoF φ ($\partial\varphi_{CD}/\partial\varphi$ and $\partial\varphi_{CD}^2/\partial\varphi^2$) and also the first and second partial derivatives of Eq. (3) ($\partial\theta_{deck}/\partial\varphi$ and $\partial\theta_{deck}^2/\partial\varphi^2$), which take a significant amount of time to calculate. These expressions reduce to linear and second-order parabolic (regardless of the degree of asymmetry) when plotted for the full range of φ i.e. from $\varphi = -\pi/2$ (representing the overturning condition in the range of negative rocking tilt of the tall pier) to $\varphi = \pi/2$ (representing the same condition in the corresponding positive range). Therefore, the complex expressions were substituted by simpler ones that depend on φ , which speed up the solution of the EoM in each time-step of the analysis; the simplified equations are not given here, for brevity, and can be found in Thomaidis (2020).

Description of the Studied Bridges

Three bridges with two rocking piers and different levels of asymmetry in their height are analyzed to establish the effect of pier irregularity on the seismic response. The height of the left pier is constant, equal to $2H_1 = 26$ m for all bridges, with the level of asymmetry being introduced through the height of the right pier (H_2) to yield: (i) a symmetric configuration with $2H_2 = 26$ m, hence $\bar{h} = 1$, (ii) a moderately asymmetric configuration with $2H_2 = 20.8$ m, hence $\bar{h} = 1.25$, and (iii) a highly asymmetric configuration with $2H_2 = 13$ m, hence $\bar{h} = 2$. In all cases, the width of the square piers is $2B = 2.6$ m. The decks consist in a continuous prestressed concrete box girder with length $L_{tot} = 2L_1 + L_2 = 2 \cdot 38 + 60 = 136$ m, depth $2h = 1.7$ m, width of the bottom and the top slabs $B_{bot} = 6$ m and $B_{top} = 9.5$ m, respectively, and flange and wall thicknesses $t_f = 0.3$ m and $t_w = 0.8$ m, respectively. With these dimensions the cross-section area of the deck is $A_{deck} = 6$ m². The bridges are built on soil type C according to the European Seismic Code EN-19981 (CEN 2004) in a seismicity zone with PGA equal to 0.36 g.

Table 1 provides further details of each bridge analyzed. The parameter $\gamma = m_{deck}/(m_{pier,1} + m_{pier,2})$ relates the mass of the deck to that of the piers, and it is an indicator of stability in rocking seismic response (Makris and Vassiliou 2014). The more asymmetric the bridge configuration, the higher are the values of the longitudinal influence of the abutments and the backfills (q), and (even more so) of the deck mass ratio (γ). This is favorable for the rocking stability of asymmetric bridges, and it is due to the reduction in the mass of their substructure ($m_{pier,1} + m_{pier,2}$) compared to the symmetric bridge with tall piers.

The abutment-backfill system is defined with a longitudinal spring with effective stiffness $k = 132 \text{ MN/m}$ and displacement at failure $u_{ab} = 100 \text{ mm}$ taken from the analysis presented by Kappos et al. (2007), further discussed in Thomaidis et al. (2020a) and Thomaidis (2020). A longitudinal dashpot with coefficient $c = 48 \text{ MN}\cdot\text{s/m}$ (Mylonakis et al. 2006) is introduced to account for the effect of both material and radiation damping of the backfill soil that is a typical dense sand of category C according to Eurocode 8 (CEN 2004). The springs and dashpots form a Kelvin-Voigt system activated when the joint gap closes, and the superstructure contacts the backwall.

Table 1. Information on the bridges with rocking piers of different degree of asymmetry, including the deck mass (m_{deck}), the pier masses ($m_{pier,1}$ and $m_{pier,2}$), and the total mass (m_{tot}) as well as the stabilizing factors of the superstructure mass effect (γ) and the longitudinal influence of the abutment-backfill system (q).

Degree of Asymmetry	$m_{deck} \cdot 10^4$ [kg]	$m_{pier,1} \cdot 10^4$ [kg]	$m_{pier,2} \cdot 10^4$ [kg]	$m_{tot} \cdot 10^4$ [kg]	γ [-]	$q \cdot 10^{-3}$ [m/kN]
Symmetric ($\bar{h} = 1$)	204	44	44	292	2.3	0.761
Moderately asymmetric ($\bar{h} = 1.25$)	204	44	35	283	2.6	0.771
Highly asymmetric ($\bar{h} = 2$)	204	44	22	270	3.1	0.786

A CoR value of $e = 0.6$ is used to describe pounding between the deck and the abutment backwalls, which is in line with the values of this coefficient reported by Jankowski (2007). The minimum gap sizes at each end of the superstructure are equal to 60 mm for all bridge configurations based on shrinkage, creep, temperature and prestressing requirements. However, due to the relatively large longitudinal influence of the abutment-backfill system (q) reported in Table 1, the abutment-backfill system is expected to suppress considerably the longitudinal displacement of the deck during rocking, which would not permit to properly evaluate the seismic response of bridges with rocking piers which are characterized by large displacements. For this reason, a relatively large gap size $u_{jo} = 120 \text{ mm}$ was selected for the end joints, to reduce the longitudinal effective stiffness in the closed gap stage of the systems.

Failure Criteria

The overturning failure mode occurs when a rocking pier exceeds its overturning capacity that is described by $|u_{pier,1}^{CG}| \geq B$ and $|u_{pier,2}^{CG}| \geq B$ for the tall and short rocking pier, respectively (Fig. 1). Moreover, failure of the abutment-backfill system is considered when $|u_{deck}^{CG}| \geq u_{jo} + u_{ab}$ (ultimate displacement of the abutment-backfill system exceeded). Therefore, the predominant failure mode of the asymmetric bridges is failure of the abutment-backfill

system if $B > u_{jo} + u_{ab}$, while overturning of the piers occurs if $B < u_{jo} + u_{ab}$. Both failure modes would occur simultaneously if $B = u_{jo} + u_{ab}$. In the structures analyzed here, the abutment-backfill failure always precedes pier overturning because $B = 1.3$ m, much larger than $u_{jo} + u_{ab} = 0.22$ m, as is the case in most bridges.

Rocking Response under Ground Motions

A total of ten Artificial Records (ARs) are utilized for the analyses. The ARs were generated with a view to matching the shape of the reference Eurocode 8 target spectrum (CEN 2004) but for a PGA higher than the design one. This is because the suppression of the rocking motion (q) by the abutment-backfill system makes it necessary to increase the seismic displacement demand to detect potential differences in the response of the examined configurations. To this end, the ARs were generated to match the Type 1 Eurocode 8 spectrum for site conditions C (CEN 2004) scaled to a PGA equal to 0.6 g.

Figs. 9A, B, C illustrate the peak displacements of the superstructure in the three bridges. Fig. 9A also depicts the longitudinal displacement of the deck for which contact with the abutments starts ($u_{jo} = 120$ mm, dotted line), and the ultimate longitudinal deck displacement for which the abutment-backfill system fails (220 mm, dashed line). It is observed that while the joint gaps are closed during rocking, none of the bridges fails under the strong ground motions (almost double the design one) applied. The results also indicate that the peak longitudinal displacement of the deck (u_{deck}^{CG}) is not strongly influenced by the asymmetry in the height of the piers, although the most asymmetric bridge ($\bar{h} = 2$) has the lowest demand of longitudinal displacements for six out of ten records. This may be attributed to the effect of the larger stabilizing factors of the deck effect (γ) and the effect of the abutment-backfill system on the longitudinal rocking motion (q) shown in Table 1, as \bar{h} increases. This result expands the finding of the study of Dimitrakopoulos and Giouvanidis (2015) that the degree of pier asymmetry does not affect the rocking response, by establishing that this applies regardless of the effects of the end supports. From the seismic performance point of view, it is observed that the symmetric bridge reaches the largest value of its capacity against the governing failure mode (i.e., failure of the abutment-backfill system), which is around 46% for AR6, while in the moderately and highly asymmetric systems the corresponding values are 44.5% and 42%, respectively, i.e. very similar to those for the symmetric bridge.

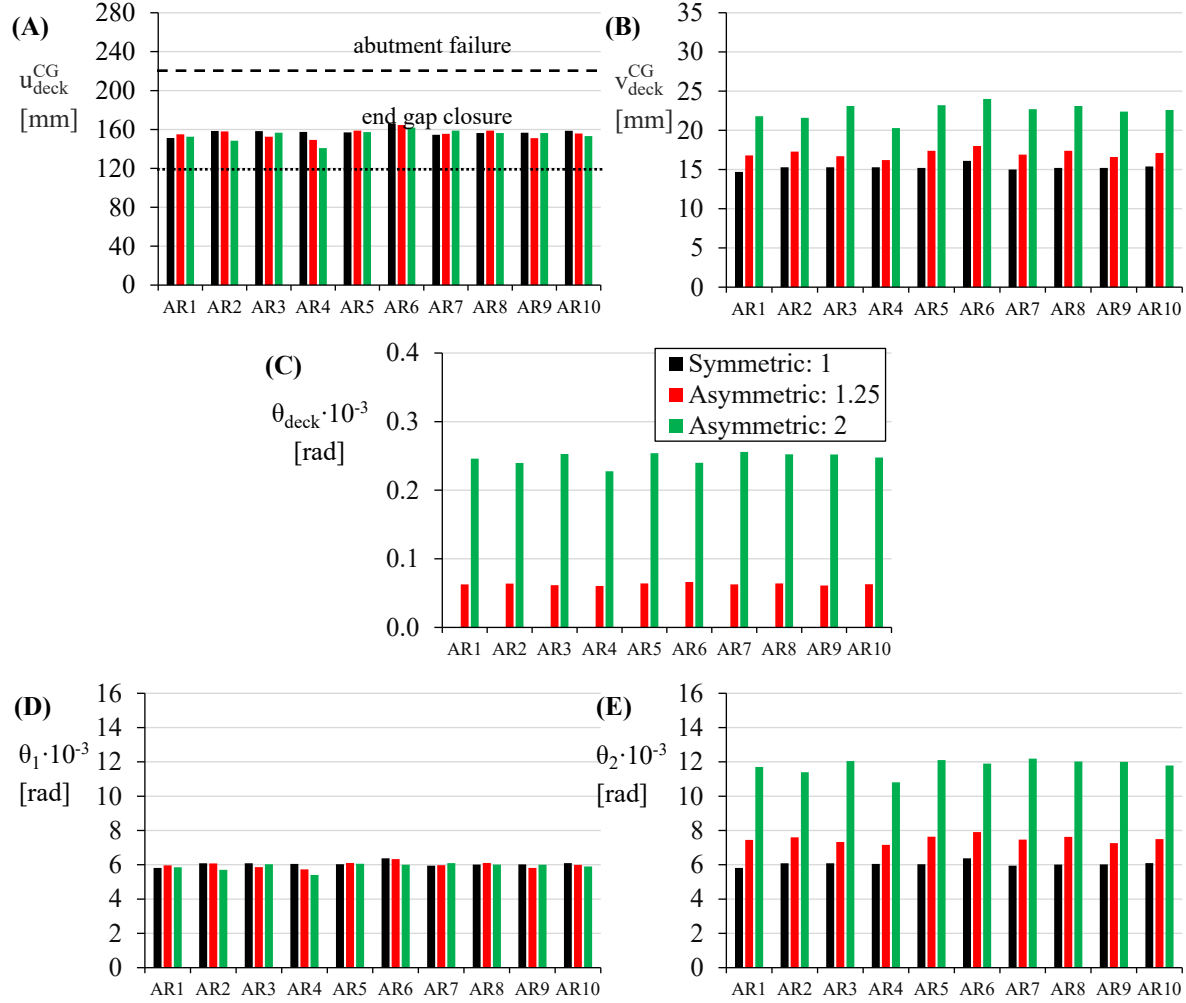


Fig. 9. Peak responses of the: (A) longitudinal (u_{deck}^{CG}) and (B) vertical displacements of the superstructure (v_{deck}^{CG}); (C) superstructure rotation (θ_{deck}); (D) relative rotation of the left rocking pier (θ_1) and (E) relative rotation of the right rocking pier (θ_2) for the bridges with rocking piers of different degrees of asymmetry.

Fig. 9B shows that the more unsymmetrical the configuration, the larger is the maximum uplift of the deck, with values of v_{deck}^{CG} in the moderately and highly asymmetric systems that are up to 14% and 52% larger than those of the symmetric structure, respectively. This can be explained by the rotation of the superstructure (θ_{deck}) shown in Fig. 9C, which is zero in the symmetric structure because the top of the two piers have exactly the same synchronous longitudinal movements, and it increases significantly with the level of asymmetry; the peak deck rotations are 0.07 and 0.26 rad for the moderately and highly asymmetric bridges subject to the AR6 and AR7 accelerograms, respectively. The unequal rotation of the piers (θ_1 and θ_2) shown in Figs. 9D, E increases significantly the vertical movement (v_{deck}^{CG}) of the deck in asymmetric rocking bridges (Fig. 9B); introducing pier asymmetry $\bar{h} = 1.25$ and 2 results in increments of v_{deck}^{CG} of 17% and 50% compared to the demand in the symmetric bridge, respectively, which

needs to be considered in the design of the abutment supports (e.g., by allowing uplift through appropriate bearings). This effect is mostly due to the larger rotation of the short pier (θ_2), with the rotation of the tall pier (θ_1) being almost unaltered.

To further explore the effect of asymmetry on the rocking behaviour, Fig. 10 shows the response histories of the superstructure and the piers for the three different bridge configurations subjected to the ground motion AR7. It is noted that the start of the rocking motion in the highly asymmetric bridge ($\bar{h} = 2$) is delayed with respect to that in other structures, which can be explained from the discussion about the effect of \bar{h} on $\ddot{u}_{g,\min}$ in Fig. 3. For this record, the symmetric bridge starts rocking at $t \approx 5.5$ s ($\ddot{u}_{g,\min} = 0.10g$), the moderately asymmetric structure at 6 s ($\ddot{u}_{g,\min} = 0.13g$), and the highly asymmetric bridge at $t \approx 7$ s ($\ddot{u}_{g,\min} = 0.15g$), when the other two bridges develop longitudinal movements that are able to close the end joint gaps and engage the abutment backwalls in the response (see dotted line in Fig. 10A). After rocking evolves, as can be seen in Fig. 10A, the superstructure moves longitudinally in a similar way for all bridge configurations for the remainder of the ground motion, showing similar amplitudes and the same number of rocking cycles. Therefore, the longitudinal behaviour of the superstructure is hardly affected by the bridge asymmetry.

Figs. 10B and C further confirm that the irregular structures present substantially larger vertical deck displacements (v_{deck}^{CG}) and deck rotations (θ_{deck}) than the symmetric bridge. As expected, this is more significant in the highly asymmetric configuration due to the differential rotations of its two piers. Figs. 10D, E show the histories of the rocking rotations of the two piers θ_1 and θ_2 , respectively, and it is seen that the tall rocking pier (whose height remains constant) has almost the same response at each rocking cycle regardless of the height of the short pier. However, reducing the height of a pier increases significantly its rotation at each rocking cycle, reaching rotational demand that is up to 140% larger than that in the piers of the symmetric bridge at $t \approx 12$ s. Nevertheless, the rocking movement attenuates faster in asymmetric structures thanks to the higher energy dissipation introduced by the impacts at the rocking interfaces, which is particularly clear after $t \approx 24$ s. This is explained by the lower values of the CoR η (which are equal to 0.986, 0.982 and 0.96 in the symmetric, moderately, and highly asymmetric bridges in Fig. 7, respectively), and by the slightly higher influence of the abutment-backfill system in the longitudinal movement (q , see Table 1). Finally, it is observed that the irregularity in pier height reduces the number of impacts during the earthquake, which can improve the structural integrity of the rocking interfaces in the bridge (e.g., Mathey et al. 2016).

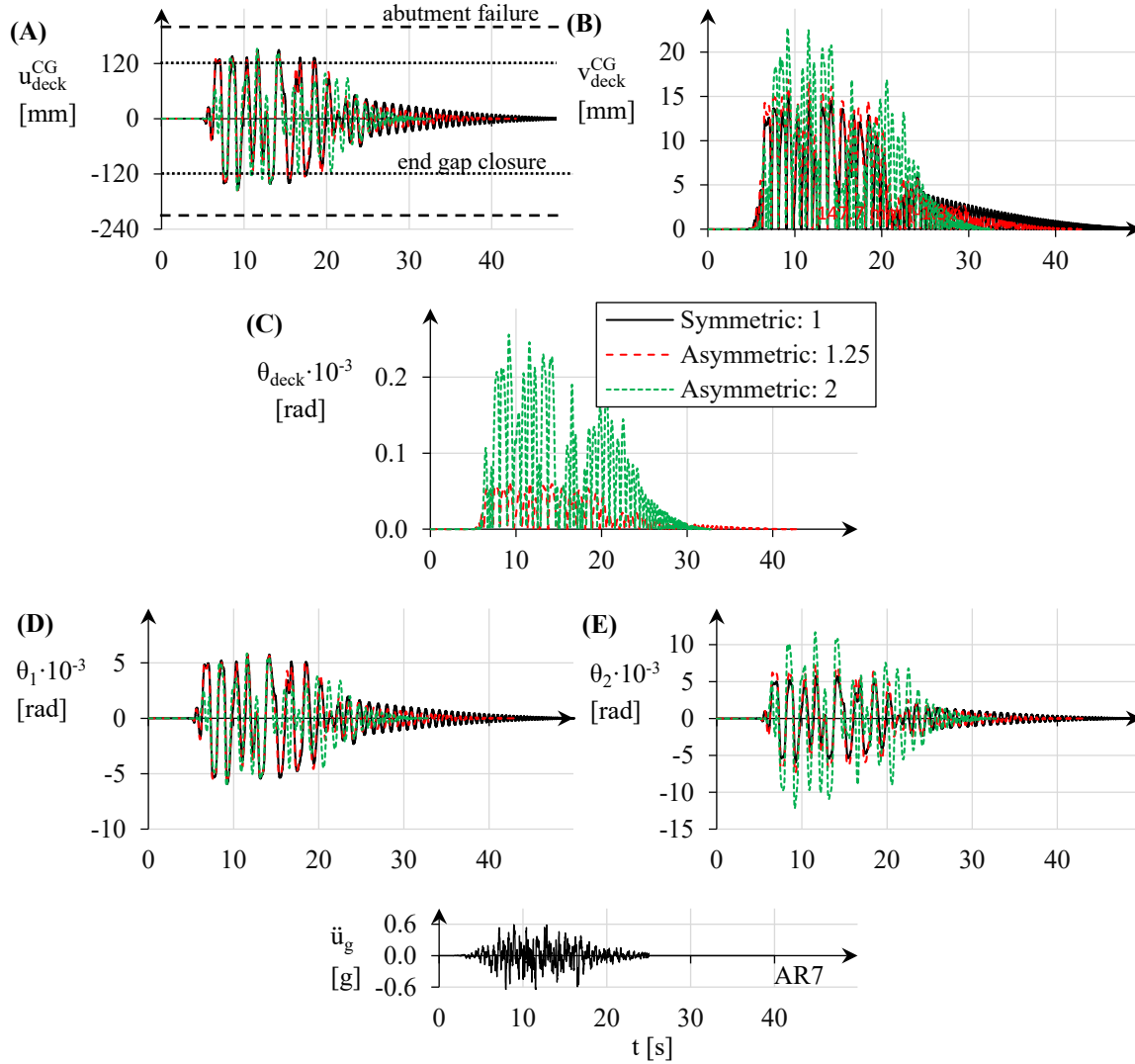


Fig. 10. Histories of the: (A) longitudinal (u_{deck}^{CG}) and (B) vertical displacements of the superstructure (v_{deck}^{CG}); (C) superstructure rotation (θ_{deck}); (D) relative rotation of the left rocking pier (θ_1) and (E) relative rotation of the right rocking pier (θ_2) for the bridges with rocking piers of different degrees of asymmetry. Results obtained when subject to AR7.

CONCLUSIONS

A new analytical model was developed to capture the rocking response of bridges with unequal pier heights, including in the formulation the end joint gaps and the abutment-backfill system. The expressions to describe initiation of rocking motion, movement during rocking, and impact at the rocking interfaces were derived based on the assumptions of (i) rigid body dynamics and (ii) avoidance of pier end sliding throughout the rocking movement; it is noted that both assumptions have been found to be fairly accurate for the rocking movement described herein. A key novelty of the analytical model is the treatment of the energy dissipation due to pounding of the superstructure on the abutment backwall through a CoR value based on the conservation of momentum.

The first part of the analysis showed that the deck supports at the abutments of asymmetric structures do not affect the magnitude of the ground acceleration that initiates rocking, so long as the abutments do not restrain the longitudinal movement of the superstructure (open end joint). A general form of the EoM for asymmetric rocking bridges was developed, which includes a term that is not present in corresponding rocking frames without end supports and expresses the stiffness and damping of the backfill when the longitudinal end joint gap is closed. A parameter q was introduced that includes the masses of the bridge components and represents the level of longitudinal resistance of the abutment-backfill. Moreover, a new expression for describing the impact at the rocking interfaces was derived, accounting for the vertical impulses developed at the abutment seats, and for different span lengths. Application of these expressions showed that the vertical supports at the abutment seats increase the value of the CoR at the rocking interfaces (η), leading to lower energy dissipation by the bridge compared to the corresponding frame without end supports. This is more significant for higher degree of asymmetry in the pier heights. Arguably, the most critical finding in a design context is that for both symmetric and unsymmetric bridge configurations the critical failure mode is not overturning of the piers (that was the focus of the bulk of previous analytical studies of rocking bridges) but rather the failure of the abutment-backfill system due to large longitudinal displacements of the deck.

The seismic response of rocking bridges with different levels of asymmetry in the pier height was studied using the developed analytical model. The results reveal that bridges with rocking piers resisted a high seismic excitation ($\text{PGA} = 0.60 \text{ g}$, almost double that of the design seismic action) with a significant reserve capacity against the prevailing failure mode (i.e., failure of the abutment-backfill system); this reserve capacity is slightly higher in the more asymmetric structures. Importantly, so long as the critical assumptions made are valid (in particular that sliding does not occur during rocking) overturning of rocking pier is not an issue. It was also observed that reducing the height of one of the piers, hence reaching a more asymmetric configuration, increases significantly its rotation demand during the rocking motion and also the rotation and the uplift of the deck; importantly, however, it does not increase the longitudinal displacement demand of the bridge. Furthermore, the response-histories of the bridges showed that structures with higher level of asymmetry experience less impacts during the rocking motion due to the delay in the initiation of the rocking motion, and the slightly higher attenuation of this motion. The latter is explained because asymmetric bridges have a slightly lower CoR at the rocking interfaces (η) and higher levels of participation of the abutment/backfill (q). Finally, it should be noted that the uplift of the deck at the abutments of bridges with rocking piers with unequal height should be duly accommodated in design; one option is to use end bearing that allow this

uplift, e.g. with concave surfaces (as in friction pendulum bearings). If this uplift is prevented (by a proper design of the anchorage of the bearings) the rocking response will be different from that described herein.

REFERENCES

- Acikgoz, S., and DeJong, M.J. (2014). "The rocking response of large flexible structures to earthquakes." *Bulletin of Earthquake Engineering*, 12, 875-908.
- Agalianos, A., Psychari, A., Vassiliou, M.F., Stojadinovic, B., and Anastasopoulos, I. (2017). "Comparative assessment of two rocking isolation techniques for a motorway overpass bridge." *Frontiers in Built Environment*, 3(47), 1-19.
- Bachmann, J.A., Strand, M., Vassiliou, M.F., Broccardo, M., and Stojadinovic, B. (2018). "Is rocking motion predictable?." *Earthquake Engineering and Structural Dynamics*, 47, 535-552.
- Ceh, N., Jelenic, G., and Bicanic, N. (2018). "Analysis of restitution in rocking of single rigid blocks." *Acta Mechanica*, 229, 4623-4642.
- CEN (2004). "Eurocode 8: Design of structures for earthquake resistance – Part 1: General rules, seismic actions and rules for buildings (EN1998-1)." *Comité Européen de Normalisation*, Brussels, Belgium.
- Chatzis, M.N., and Smyth, A.W. (2012a). "Modeling of the 3D rocking problem." *International Journal of Non-linear Mechanics*, 47, 85–98.
- Chatzis, M.N., and Smyth, A.W. (2012b). "Robust modeling of the rocking problem." *Journal of Engineering Mechanics*, 138(3), 247-262.
- Cheng, C-T. (2007). "Energy dissipation in rocking bridge piers under free vibration tests." *Earthquake Engineering and Structural Dynamics*, 36, 503-518.
- DeJong, M.J., and Dimitrakopoulos, E.G. (2014). "Dynamically equivalent rocking structures." *Earthquake Engineering and Structural Dynamics*, 43, 1543-1563.
- Di Egidio, A., and Contento, A. (2009). "Base isolation of slide-rocking non-symmetric rigid blocks under impulsive and seismic excitations." *Engineering Structures*, 31, 2723-2734.
- Dimitrakopoulos, E.G., and DeJong, M.J. (2012). "Overturning of retrofitted rocking structures under pulse-type excitations." *Journal of Engineering Mechanics*, 138, 2294-2318.
- Dimitrakopoulos, E.G., and Giouvanidis, A.I. (2015). "Seismic response analysis of the planar rocking frame." *Journal of Engineering Mechanics*, 141(7), 04015003.
- Drosos, V.A., and Anastasopoulos, I. (2014). "Shaking table testing of multi-drum columns and portals." *Earthquake Engineering and Structural Dynamics*, 43, 1703-1723.
- ElGawady, M.A., Ma, Q., Butterworth, J.W., and Ingham, J. (2011). "Effects of interface material on the performance of free rocking blocks." *Earthquake Engineering and Structural Dynamics*, 40, 375-392.
- Housner, G.W. (1963). "The behavior of inverted pendulum structures during earthquakes." *Bulletin of the Seismological Society of America*, 53(2), 403-417.
- Jankowski, R. (2007). "Theoretical and experimental assessment of parameters for the non-linear viscoelastic model of structural pounding." *Journal of Theoretical and Applied Mechanics*, 45(4), 931-942.
- Jeong, M.J., Suzuki, K., and Yim C-S. (2003). "Chaotic rocking behaviour of freestanding objects with sliding motion." *Journal of Sound and Vibration*, 262, 1091–1112.
- Kalliontzis, D., Sritharan, S., and Schultz, A. (2016). "Improved coefficient of restitution estimation for free rocking members." *Journal of Structural Engineering*, 142(12).
- Kappos, A.J., Potikas, P., and Sextos, A.G. (2007). "Seismic assessment of an overpass bridge accounting for non-linear material and soil response and varying boundary conditions." *Conference: ECCOMAS Thematic Conference on Computational Methods in Structural Dynamics and Earthquake Engineering*, Rethymno, Greece.
- Makris, N., and Kampas, G. (2016). "Size versus slenderness: Two competing parameters in the seismic stability of free-standing rocking columns." *Bulletin of the Seismological Society of America*, 106(1).

597 Makris, N., and Roussos, Y. (2000). "Rocking response of rigid blocks under near-source ground motions."
598 *Geotechnique*, 50(3), 243-262.

599 Makris, N., and Vassiliou, M.F. (2013). "Planar rocking response and stability analysis of an array of free-standing
600 columns capped with a freely supported rigid beam." *Earthquake Engineering and Structural Dynamics*, 42, 431-
601 449.

602 Makris, N., and Vassiliou, M.F. (2014). "Are some top-heavy structures more stable?." *Journal of Structural*
603 *Engineering*, 140(5), 06014001.

604 Makris, N., and Zhang, J. (2001). "Rocking response of anchored blocks under pulse-type motions." *Journal of*
605 *Engineering Mechanics*, 127(5), 484-493.

606 Mathey, C., Feau, C., Politopoulos, I., Clair, D., Baillet, L., and Fogli, M. (2016). "Behavior of rigid blocks with
607 geometrical defects under seismic motion: An experimental and numerical study." *Earthquake Engineering and*
608 *Structural Dynamics*, 45, 2455-2474.

609 MATLAB (2016). "Version 9.1.0.441655 (R2016)." Natick, Massachusetts: The MathWorks Incorporation.

610 Muthukumar, S., and DesRoches, R. (2006). "A Hertz contact model with non-linear damping for pounding
611 simulation." *Earthquake Engineering and Structural Dynamics*, 35, 811-828.

612 Mylonakis, G., Nikolaou, S., and Gazetas, G. (2006). "Footings under seismic loading: Analysis and design issues
613 with emphasis on bridge foundations." *Soil Dynamics and Earthquake Engineering*, 26, 824-853.

614 Psycharis, I., Papastamatiou, D., and Alexandris, A. (2000). "Parametric investigation of the stability of classical
615 columns under harmonic and earthquake excitations." *Earthquake Engineering and Structural Dynamics*, 1093-
616 1110.

617 Roh, H.S., and Reinhorn, A.M. (2010). "Nonlinear static analysis of structures with rocking columns." *Journal of*
618 *Structural Engineering*, 135(5), 532-542.

619 Shi, Z., and Dimitrakopoulos, E.G. (2017). "Comparative evaluation of two simulation approaches of deck-abutment
620 pounding in bridges." *Engineering Structures*, 148, 541-551.

621 Taniguchi, T. (2002). "Non-linear response analyses of rectangular rigid bodies subjected to horizontal and vertical
622 ground motion." *Earthquake Engineering and Structural Dynamics*, 31, 1481-1500.

623 Thiers-Moggia, R., and Málaga-Chuquitaype, C. (2018). "Seismic protection of rocking structures with inerters."
624 *Earthquake Engineering and Structural Dynamics*, 48, 528-547.

625 Thomaidis, I.M. (2020). "Analytical and numerical investigation of the seismic behaviour of bridges with rocking
626 piers." *Thesis (PhD)*, City, University of London, London, UK.

627 Thomaidis, I.M., Camara, A., and Kappos, A.J. (2018). "Simulating the rocking response of rigid bodies using general-
628 purpose finite element software." *Conference: 16th European Conference on Earthquake Engineering*,
629 Thessaloniki, Greece.

630 Thomaidis, I.M., Kappos, A.J., and Camara, A. (2020a). "Dynamics and seismic performance of rocking bridges
631 accounting for the abutment-backfill contribution." *Earthquake Engineering and Structural Dynamics*, 49(12),
632 1161-1179.

633 Thomaidis, I.M., Kappos, A.J., and Camara, A. (2020b). "Rocking vs Conventional seismic isolation: Comparative
634 assessment of asymmetric bridges in a design context." *Conference: 17th World Conference on Earthquake*
635 *Engineering*, Sendai, Japan.

636 Vassiliou, M.F. (2017). "Seismic response of a wobbling 3D frame." *Earthquake Engineering and Structural*
637 *Dynamics*, 1-17.

638 Vassiliou, M.F., and Makris, N. (2012). "Analysis of the rocking response of rigid blocks standing free on a seismically
639 isolated base." *Earthquake Engineering and Structural Dynamics*, 21, 177-196

640 Vassiliou, M.F., and Makris, N. (2015). "Dynamics of the vertically restrained rocking column." *Journal of*
641 *Engineering Mechanics*, 2015, 141(12), 04015049.